Design, Fabrication, Testing and Modeling of a Vaporizing Liquid Micro-Propulsion System

van Wees, T.; Hanselaar, Caspar; Jansen, E; Cervone, Angelo; Zandbergen, Barry; van Zeijl, Henk

Publication date
2016

Document Version
Accepted author manuscript

Published in
Space propulsion 2016

Citation (APA)
van Wees, T., Hanselaar, C., Jansen, E., Cervone, A., Zandbergen, B., & van Zeijl, H. (2016). Design, Fabrication, Testing and Modeling of a Vaporizing Liquid Micro-Propulsion System. In *Space propulsion 2016* Article SPC2016_3124914

SPC2016_3124914

DESIGN, FABRICATION, TESTING AND MODELING OF A VAPORIZING LIQUID MICROPROPULSION SYSTEM

T. van Wees[(1)], C. Hanselaar[(2)], E. Jansen[(3)], I. Granero[(4)], A. Cervone[(5)], B. Zandbergen[(6)], H. Van Zeijl[(7)]

[(1)]Delft University of Technology Faculty of Aerospace Engineering, Kluyverweg 1, 2629HS Delft, The Netherlands, Email: tiemenvwees@hotmail.com
[(2)]Delft University of Technology Faculty of Mechanical Engineering, Mekelweg 2, 2628CD Delft, The Netherlands, Email: caspar.hanselaar@me.com
[(3)]Delft University of Technology Faculty of Aerospace Engineering, Kluyverweg 1, 2629HS Delft, The Netherlands, Email: edward.hwj@gmail.com
[(4)]Delft University of Technology Faculty of Aerospace Engineering, Kluyverweg 1, 2629HS Delft, The Netherlands, Email: nach_g3m@hotmail.com
[(5)]Delft University of Technology Faculty of Aerospace Engineering, Kluyverweg 1, 2629HS Delft, The Netherlands, Email: A.Cervone@tudelft.nl
[(6)]Delft University of Technology, Faculty of Aerospace Engineering, Kluyverweg 1, 2629HS Delft, The Netherlands, Email: B.T.C.Zandbergen@tudelft.nl
[(7)]Delft University of Technology, Else Kooi Laboratory, Feldmannweg 17, 2628CT Delft, The Netherlands, Email: H.W.vanZeijl@tudelft.nl

ABSTRACT

In the last decade, CubeSat development has shown the potential to allow for low-risk, low-cost space missions. To further improve the capabilities of CubeSats in large scale missions, a novel micro-propulsion system is being developed at Delft University of Technology. The system is based on a Vaporizing Liquid Microthruster (VLM), which is manufactured by means of Micro Electro-Mechanical Systems (MEMS) technology. It aims to achieve a specific impulse of 100 s and thrust of 1.4 mN, using water as propellant. This paper presents a status update of the development project. Design solutions are shown to circumvent manufacturing tolerances in the wafer-bonding and sealing of the interfaces of the VLM. Secondly, performance analysis based on a 1D-flow approximation is shown to provide a useful tool to quickly predict VLM performance. Next, a detailed design of the propellant storage tank for the CubeSat micro-propulsion system is presented. Finally, the test plan and test setup for the VLM are elaborated, presenting solutions to determine chamber temperature and pressure without directly sensing it.

GLOSSARY

Symbol	Unit	Description
Δp	Pa	Pressure loss
Δx	m	Section length
Γ	-	Vandenkerckhove function
ϵ	-	Volume fraction remaining with pillars
η	-	Nozzle efficiency
κ	$W \cdot m^{-1} \cdot K^{-1}$	Conductivity of fluid
μ	Pa·s	Viscosity of fluid
ρ	$kg \cdot m^{-3}$	Density of fluid
τ	s	Residence time
Φ_S	-	Sphericity of fluid
A_{cs}	m^2	Local cross-sectional area
A_e	m^2	Exit area
A_t	m^2	Throat area
C_D	-	Discharge coefficient
C_{tp}	-	Two-phase heat transfer correlation coefficient
D_h	m	Hydraulic diameter
D_p	m	Hydraulic diameter of pillar
F	N	Thrust force
f	-	Friction factor
g_0	$m \cdot s^{-2}$	Gravitional acceleration
h_{conv}	$W \cdot m^{-2} \cdot K^{-1}$	Convective heat transfer coefficient
I_{sp}	S	Specific impulse
i	-	Section counter
L	M	Length
$\dot{m}$	$kg \cdot s^{-1}$	Mass flow
Nu	-	Nusselt number
n	-	Number of sections
P	W	Power

P_w	M	Wetted perimeter
p_c	Pa	Chamber pressure
p_e	Pa	Nozzle exit pressure
Q	W	Heat transfer
R_s	$J \cdot kg^{-1} \cdot K^{-1}$	Specific gas constant
Re	-	Reynolds number
T	K	Local temperature
T_c	K	Chamber temperature
T_w	K	Wall temperature
u	$m \cdot s^{-1}$	Local velocity
u_e	$m \cdot s^{-1}$	Exit velocity
u_s	$m \cdot s^{-1}$	Superficial velocity

1 INTRODUCTION

In order to make access to space cheaper, faster and easier, miniaturization is essential in space engineering. In the last decade, small satellites such as CubeSats have shown great success for education and low-cost experiments [1]. Recently, they are proposed for more ambitious applications, such as Earth observation [2], space debris mitigation and scientific missions [3]. However, most Cubesats flown presently lack an active propulsion system, limiting their orbital lifetime and maneuverability. In order for small satellites to become more relevant to these ambitious large scale missions, miniaturized propulsion is therefore essential.

Previously, the design of a vaporizing liquid micro-thruster (VLM), manufactured through MEMS-technology, has been presented [4]. Using water as propellant, a specific impulse of 100 s and thrust of up to 1.4 mN is targeted. The MEMS-VLM thruster builds on earlier work performed on a nitrogen propelled micro-resistojet [5, 6]. A system overview of the full VLM propulsion system has been described in [7].

This paper presents updates on design, manufacturing and test of the various components of the micro-propulsion system. First of all, this paper shows the fabrication results of the MEMS-VLM. Design solutions are presented that solve misalignment in the MEMS fabrication process, failing of the electrical contacts and leakage through electrical contact openings.

Secondly, performance modelling is presented using analytical methods for boiling flow. This analysis uses a steady-state 1D flow approximation, correlated to published VLM performance data. The applied nozzle flow calculations are adjusted for slit-nozzles, providing a useful tool to quickly predict VLM performance.

Furthermore, the detailed design of the propellant storage system is shown, along with stress analysis using Finite Element Methods.

Finally, a summary of the test plan and test setup for the VLM are presented along with conclusions resulting from the work performed so far.

2 SUMMARY OF THE DESIGN

The design of the VLM has previously been presented in [4, 8] while the overview of the complete micro-propulsion system is presented in [7]. The work presented in this paper builds on those works and is summarized in this section.

The driving requirements for the micro-propulsion system are [4]:

- The total Delta-V provided shall be at least 15 $m \cdot s^{-1}$ to a 3.6 kg CubeSat.
- The thrust shall be between 0.5 mN and 9.5 mN.
- The wet mass at launch shall not exceed 459 g.
- The dimensions shall not exceed 90x90x80 mm.
- The peak power consumption shall not exceed 10 W.
- The internal pressure shall not exceed 10 bar.

The micro-propulsion system is divided into a thruster (the VLM), a propellant tank, a feed system and supporting electronics. The latter two are based on Commercial-Off-The-Shelf (COTS) components, as is described in [7], while the propellant tank design is reported in Section 4.

The VLM design consists of an inlet channel, a heating chamber and a nozzle, see Fig. 1. Mirror images of each of these components are etched in two wafers, after which these wafers are bonded to enclose the flow channels. The heating chamber has a flat, rectangular cross-section, where heater wires are suspended traverse to the flow direction in the center of the chamber. These heater wires are supported by diamond-shaped pillars, as is shown in Fig. 2.

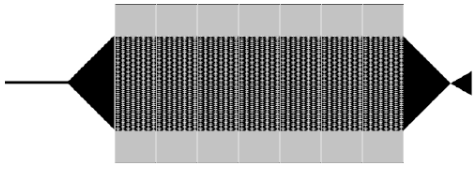

Figure 1. Schematic of the VLM-design. The inlet is shown on the left, seven sections of heating chamber in the center and the nozzle on the right.

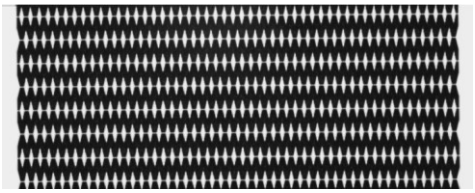

Figure 2. Close up of a heater section. The SiC-heaters are shown in gray, while the depth of the flow channel is shown in black.

3 MANUFACTURING

Manufacturing of the VLM as designed in [4] has taken place in the Else Kooi Laboratory for MEMS. Here, the design changes that have resulted as a consequence of manufacturability are presented, along with the manufacturing flow.

The wafer processing flow is best described following Fig. 3. The result is two wafers with mirror images of the flow channels and nozzle, with a heater stack on one wafer and a pocket on the other to fit the heater stack. These wafers are bonded through fusion bonding, after which holes are etched through the top wafer to connect electrical and fluidic interfaces.

a. Silicon wafer

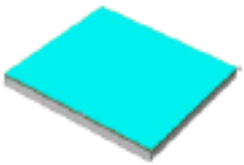

b. Deposit heater stack (SiO2 – SiC – SiO2)

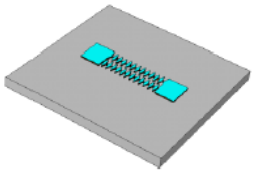

c. Etch heater geometry

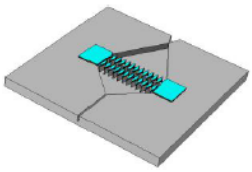

d. Etch flow channels Anisotropic DRIE > isotropic DRIE*

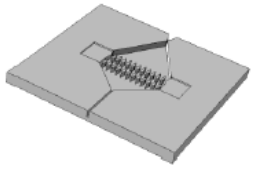

e1. Old capping wafer (similar process as d.)

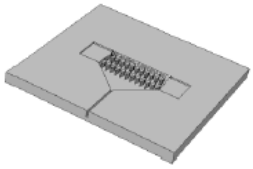

e2. New capping wafer (similar process as d.)

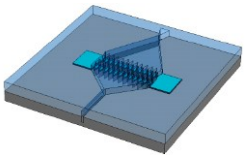

f1. Wafer bonding (old design)

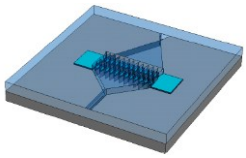

f2. Wafer bonding (new design)

*Figure 3. Schematic summary of the wafer processing. *DRIE: Deep Reactive Ion Etching*

Fig. 4 shows a Scanning Electron Microscope (SEM) image of the nozzle in the original design (Fig. 3-e1 and -f1). Significant misalignment in the wafer bonding is apparent in the first attempt. This is avoided by a redesign of the nozzle, where the nozzle is not etched in the capping wafer (Fig. 3-f1 and --f2). In the other wafer, the throat is widened in order to reach the appropriate throat size. A SEM-image of the new nozzle is shown in Fig. 5. The reduction in area ratio from 20 down to 11, as a consequence of this design change, is estimated to yield a performance loss of 4% [8].

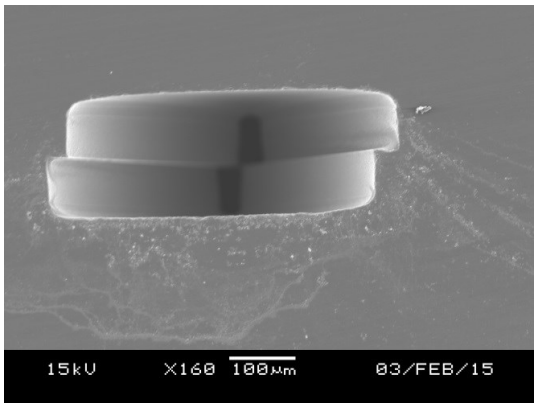

Figure 4. SEM image of the original nozzle, directed at the throat through the exit

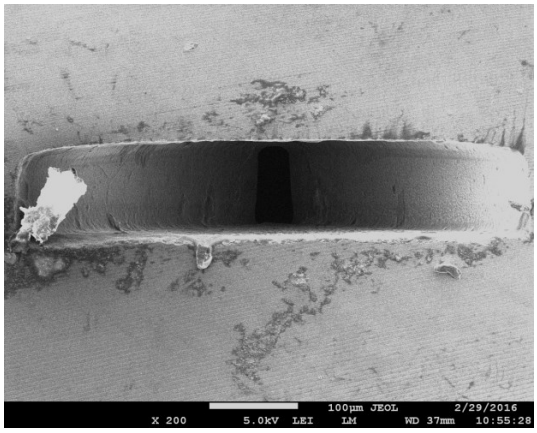

Figure 5. SEM image of the new nozzle (taken after preliminary tests, thus showing contamination)

3.1 Electrical interface

The heaters are connected by means of wire-bonding, which is done at the Advanced Packaging Center in Duiven, The Netherlands. The interfaces for wire bonding are made by etching pockets in one wafer to connect to the bond pads on the heaters. Figure 6 shows a schematic of pockets in the bottom wafer (A) and capping wafer (B), respectively.

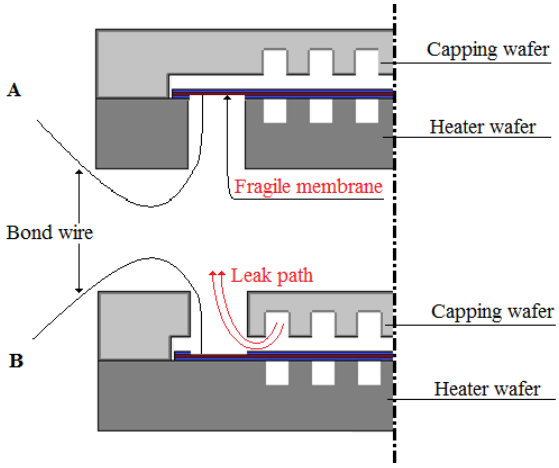

Figure 6. Schematic cross-section of the options for orientation of the bond wire interfaces

They are inherently different since the capping wafer does not touch the heater stack, leaving a slight gap. This gap can form a potential leak path which is sealed by the heater stack in option A, but not in option B. However, in orientation A the bond pads are not supported, which causes the fragile heater stack to consistently fail during wire-bonding attempts. This led to the decision to etch the pockets in the capping wafer instead (option B). As a consequence, an alternative method of sealing is required. The seals are made by flowing a low-viscosity bonding agent into the cavities after wire-bonding, the result is shown in Fig. 7. These seals are sufficient for preliminary testing up to 300^{o}C. For further development, in order to further increase the temperature a different design for the heater interfaces is recommended.

3.2 Fluid interface

The interface to supply fluid is made by connecting a fluid dispensing needle to the feed system, which is bonded to a hole etched into the capping wafer that aligns with the inlet channel in the thruster. This is shown in Fig. 7. This interface is found to be sufficient for breadboard-level testing of the VLM.

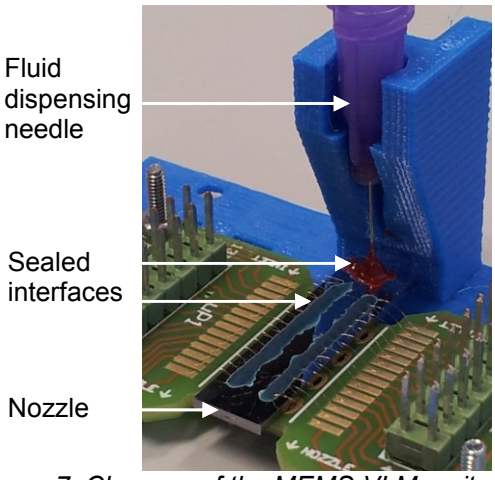

Figure 7. Close-up of the MEMS-VLM on its PCB showing seals on the wire-bonds and, fluidic interface to the thruster

4 PREDICTIVE ANALYTICAL MODEL

Numerical first principal approaches are rejected as viable simulation methods for this study, as the two- phase evaporative micro-flow simulations currently available are found not to provide the necessary accuracy and reliability to justify the increased effort in tuning and validation, as well as the increased computation time compared to analytical models.

The performance analysis therefore uses an analytical steady-state modelling approach. Fluid properties are assumed to be continuous functions of enthalpy and pressure.

Mass flow rate ($\dot{m}$) is estimated using ideal rocket theory [9, 10] as a function of chamber pressure (P_c), throat area (A_t), the Vandenkerckhove function (Γ), specific gas constant (R_s) and chamber temperature (T_c). A discharge correction factor (C_D) has been added to allow for non-ideal behavior.

$$\dot{m} = C_D \frac{p_c A_t \Gamma}{\sqrt{R_s T_c}} \tag{1}$$

The heater is divided along the direction of the flow in *n* shorter sections of length Δx. Laminar flow is assumed throughout the inflow and heating section. This will be substantiated via Reynolds number (Re) calculations in the model, using mass flow, cross section, local viscosity and hydraulic diameter. Heat (Q) is added to the fluid flow, proportional to the convective heat coefficient ($\mathrm{h_{conv}}$) and the wall and local fluid

temperature (T) of section 'i'. At section 'i = n' the fluid properties represent the chamber properties.

$$Q = C_{tp} h_{conv} (T_w - T_i) P_w \Delta x \quad (2)$$

Here, C_{tp} is a two-phase correlation factor and P_w is the wetted perimeter of the cross-section. Two-phase heat-transfer coefficients have been correlated to visual references, based on the heater-length required to fully evaporate the fluid (no more liquid visible in the flow beyond the recorded length), given the silicon wall temperature, mass flow and inflow temperature, as published by [11, 12]. By adjusting the term C_{tp}, model results are correlated to the observed experimental results. The convection coefficient is determined using eq. (3), with the Nusselt number Nu based on tabulated data [13] for laminar flows.

$$h_{conv} = Nu \frac{\kappa}{D_h} \quad (3)$$

Here, κ is the conductivity of the fluid and D_h is the hydraulic diameter. The total energy influx is calculated via eq. (2), the residence time and section length Δx, to evaluate the enthalpy in the next section. Based on the calculated local enthalpy and pressure, average fluid properties are assessed.

The pressure drop (Δp) is calculated per section, using the Kozeny-Carman relation, with μ the viscosity of the fluid, Φ_s the sphericity of the pillars in the flow, D_p the pillar hydraulic diameter, ϵ the ratio of volume left after pillars are placed over total volume without pillars and u_s the superficial velocity calculated without pillars:

$$\frac{\Delta p}{\Delta x} = \frac{180\mu}{\Phi^2 D_p^2} \frac{(1-\epsilon)^2}{\epsilon^3} u_s \quad (4)$$

Consequently using a sufficiently high number of sections (approximately 4000), the average distribution of pressure and enthalpy throughout the fluid flow is calculated.

Using this data, an insight into the minimal wall temperature needed for full evaporation is calculated for a given system length. Similarly the pressure drop and mass flow rate are predicted, providing a more reliable estimate of system performance.

Extending the projections of the system performance to include the thrust levels (F), the isentropic exit- plane velocities (u_e) and pressures (p_e) are determined using ideal rocket theory. In the computation of the final thrust, an efficiency factor η has been included to account for the significant boundary layer thickness in the nozzle, resulting in eq. (5) for the thrust in vacuum:

$$F = \eta \, (\dot{m} \cdot u_e + p_e A_e) \quad (5)$$

The specific impulse (I_{sp}) finally follows from the definition:

$$I_{sp} = \frac{F}{g_o \dot{m}} \quad (6)$$

Here, g_o is the sea-level gravitational acceleration.

4.1 Results

The results presented here are produced taking a discharge factor of $C_D = 0.7$ [14] and a nozzle efficiency of 0.85 [15]. Fig. 8a shows the progression of temperature through the heater for an inflow pressure of 2 bar and consequently a mass flow varying between 0.37 ($T_w = 680$ K) and 0.47 mg·s^{-1} (Tw = 430 K). The wall temperature appears to be sufficient to ensure evaporation in all investigated cases. However in Fig. 8b the inlet pressure of 5.0bar and mass flow rates between 0.93 (T_w = 680 K) and 1.18 mg·s^{-1} (T_w = 430 K) show that the saturation temperature (424.8 K) is too close to the wall temperature to facilitate sufficient evaporation, at a wall temperature of 430 K.

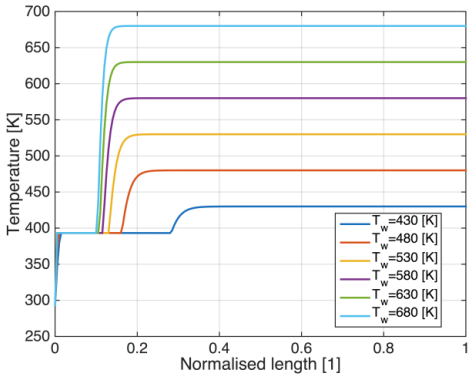

(a) $P_c = 2\ bar$

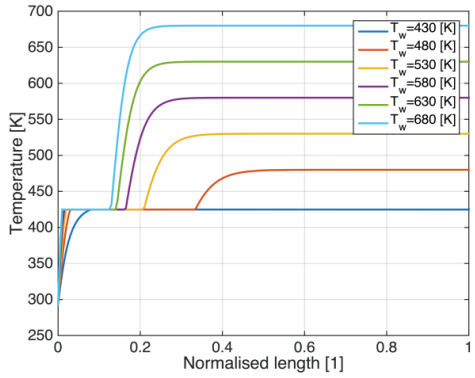

(b) $P_c = 5\ bar$

Figure 8. Temperatures of the fluid over the normalized length of the heater

In Fig. 9 the pressure drop registered over the length of the heaters is shown. Despite the flow-interrupting pillars, the pressure drop remains limited to approximately 2.5% in the 2.0 bar case and less than 1% in the 5.0 bar case. Tab. 1 substantiates this. This suggests that mass flow rate can be reasonably estimated using the inlet pressure, without the need to determine the pressure drop in the heater.

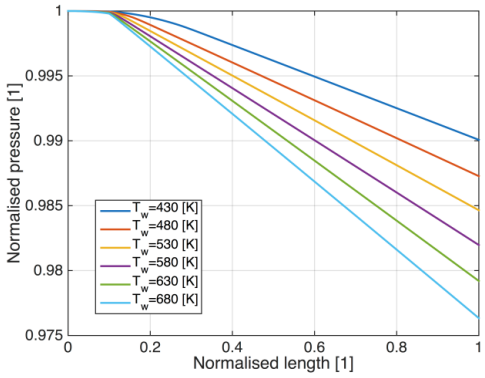

(a) $P_c = 2\ bar$

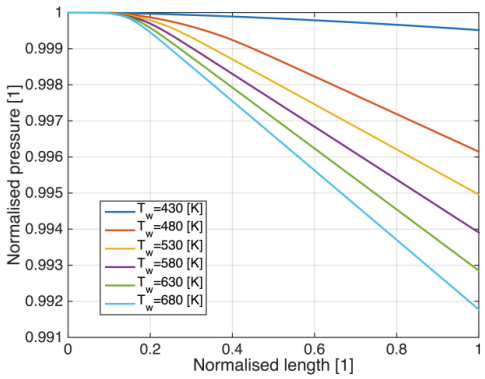

(b) $P_c = 5\ bar$

Figure 9. Normalized pressures over the normalized length of the heater

The thrust levels attained are shown in Tab. 1. The laminar flow assumption is substantiated via the Reynolds numbers, also shown in Tab. 1. Predicted values for vacuum specific impulse are given in Tab. 2.

Table 1. Inlet pressure, chamber pressure, Reynolds number range and thrust predicted

P_{in}[bar]	P_c [bar]	Re [-]	F [mN]
1.0	0.966	0.8 - 65.9	0.23
2.0	1.967	1.6 - 116	0.47
3.0	2.968	2.5 - 156	0.71
4.0	3.969	3.3 - 182	0.95
5.0	4.971	4.2 - 194	1.19

Table 2. Specific impulse values predicted

Wall temperature [K]	I_{sp} [s] eq. (6)
430	103
480	109
530	115
580	120
630	125
680	130

In conclusion, the proposed correlated analytical steady-state model allows a designer to quickly and accurately investigate minimum wall temperature requirements for a given design proposal. This provides a useful tool for quick assessments of concepts in future re-design efforts.

5 PROPELLANT TANK DESIGN

The feed- and control system design for propellant supply to the VLM are largely based on Commercial of the Shelf (COTS) components. These components have been described earlier in [7]. No COTS system is available for the storage of the VLM propellant (nitrogen pressurized liquid water). Therefore an in-house design is developed. The driving requirements for the storage tank are listed in Tab. 3.

Table 3. Driving requirements for the propellant storage tank

Parameter	Unit	Requirement
Propellant	-	Liquid water
Mass total	g	≤200
Max. geometry (WxDxH)	mm	100x100x40
Internal volume	mL	≥200
MEOP	bar	10
Acceleration load	$m \cdot s^{-2}$	+/- 5g
Eigenfrequency	Hz	>100
Safety factor on yield load	-	1.5

Based on a preliminary design trade made by I. Granero [16], the tank configuration is selected to be an aluminum box shape with one open side and is sealed off with a lid. The lid is sealed with an axially loaded rubber O-ring gasket around the edge of the lid and structurally joined to the box by using bolts as the joining method. Compliance with the structural requirements is achieved by using vertical stiffeners on the inside of the storage volume. This preliminary concept is presented in Fig. 10a.

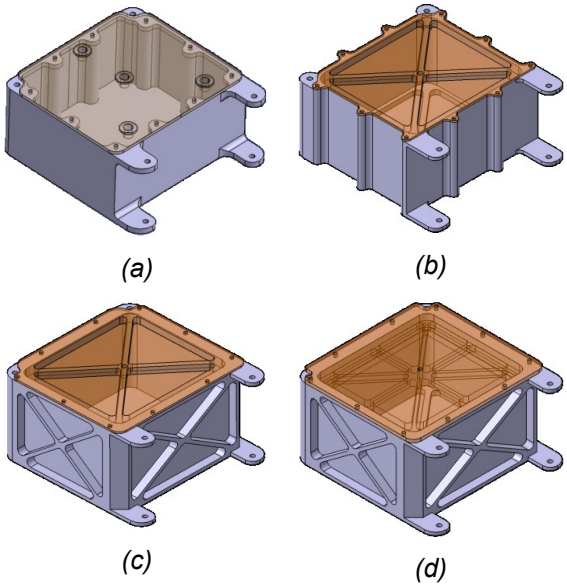

Figure 10. Iterative design steps of the VLM propellant tank.

Fig. 10 shows the iterative steps from the preliminary concept (a) towards an engineering model design (d). The first iteration (b), relocates the vertical stiffeners to the outside of the tank structure in order to allow for sealing to be applied between the inside of the box structure and the lid. Sealing is provided by means of a radial O-ring in the lid. The relocation of the vertical stiffeners results in a decrease in internal volume, thereby not complying with the 200 mL requirements. Therefore the height of the tank is increased to compensate for the loss in volume. A cross shaped stiffening method is applied to the lid to reduce mass.

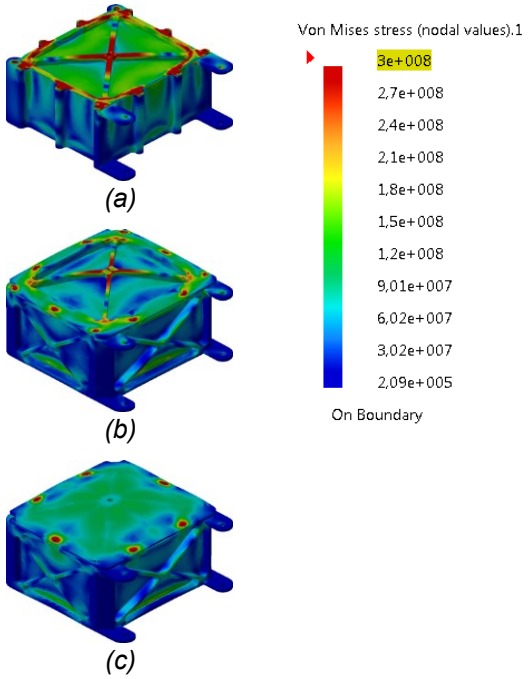

*Figure 11. Finite element analysis of the VLM propellant tank iteration**s***

CATIA V5 is used to perform Finite Element Analysis (FEA) on the stresses using the Generative Structural Analysis Toolkit. The results from this analysis are not to be interpreted as final; however they provide a good indication on the location of stress concentrations and overall structural performance. Experimental validation of the results is thus still required. The maximum value on the color scale in Fig. 11 indicates the maximum allowable stress based on a yield strength for aluminum of 300 MPa. Fig. 11a presents the FEA result of the first iteration step (Fig. 10b) when subjected to an internal pressure of 10 bar. Large stress concentrations are present in this design on the lid and the connection points of the lid to the box structure.

The design step shown in Fig. 10c, corresponding to the FEA in Fig. 11b, reduces the stress concentrations on the lid connection points by increasing the available surface area around the bolts. Furthermore the vertical stiffeners are replaced with cross-shaped stiffeners to enable further reduction in tank mass.

The final design step presented in Fig. 10d relocates the stiffeners from the outside of the lid to the inside of the lid in order to comply with the structural requirements.

Furthermore, the stiffener configuration on the lid is altered for a more mass optimized design. The FEA results shown in Fig. 11c still indicate too high stresses acting on the bolt connections. These can be contributed to the application of fixated virtual bolts in the FEA. Fig. 12 presents a FEA of the stresses present in the joining connection when physical steel bolts and nuts are used as joining method. Fig. 12 shows the loads carried by the bolt/nut connection instead of the tank/lid interface.

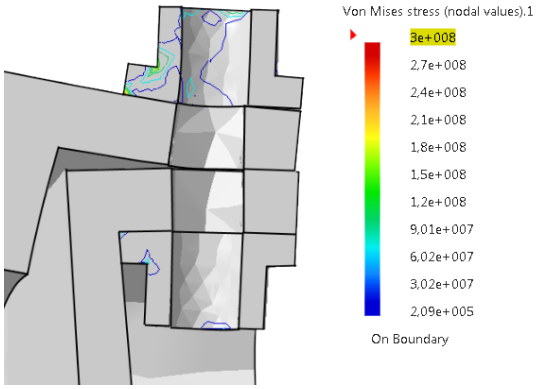

Figure 12. Propellant tank bolt/nuts connection FEA detail (deformation not to scale)

Tab. 4 presents the changes in the tank characteristics from the preliminary design to the engineering model design.

Table 4. Propellant tank requirement compliance

Parameter	Unit	Requirement	Preliminary design	Engineering model design
Mass Lid	g	-	68	67
Mass Tank	g	-	135	160
Mass total	g	≤200	203	227
Max. geometry (WxDxH)	mm	100x100x40	90x96x41	90x96x49.5
Internal volume	mL	≥200	231	237
MEOP	bar	10	X	✓
Acceleration load	$m \cdot s^{-2}$	+/- 5g	✓	✓
Eigenfrequency	Hz	>100	N/A	>1636

6 TEST PLAN AND SETUP

Testing so far is focused on the functionality of the heating chamber and nozzle of the VLM. The approach for testing is bottoms up, where the quality of individual components is determined first, followed by functional tests and completed by performance tests. On the highest level, the test plan includes the following seven steps:

1. Optical characterization of the heater and nozzle geometry to determine critical dimensions.
2. Electrical characterization of the heaters by measuring their IV-behavior.
3. Leak testing of the thruster and feed system.
4. Testing of the power supply- and measurement circuits.
5. Determination of nozzle performance in cold gas mode.
6. Determination of heater performance in hot gas mode.
7. Determination of heater performance in boiling flow mode.

These steps are elaborated on hereafter. However, since the optical characterization was described previously in [4], this will not be elaborated on here.

6.1 Electrical characterization

The heaters are characterized in a wafer probing station by supplying a range of voltages from -40 V to +40 V and measuring the current entering the heater, leaving the heater and leaking through the silicon. Typical IV-curves for the seven heaters in one thruster are shown in Fig. 13. They show consistent nearly linear resistance behavior as long as a positive potential is supplied. Furthermore, the effect of heating is apparent as the gradient of the IV-curve increases slightly when power increases.

The heater current is found to leak excessively through the silicon in case negative potentials are supplied, indicating diode-like behavior of the insulation layer. This is easily circumvented by ensuring positive potentials while the thruster is electrically grounded.

Finally, of the 210 heaters that have been characterized, 23 were found to fail at least partially. These failures include current leaks (6), partially broken heaters found to have significantly higher resistance than expected (10) and completely broken heaters (7). This indicates limited reliability in the manufacturing of these heaters, stressing the need to repeat this measurement on every produced thruster.

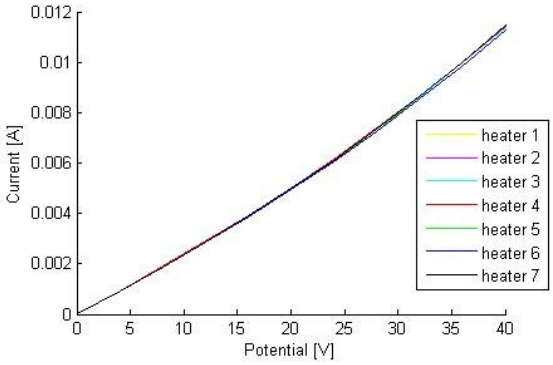

Figure 13. Typical IV curves of seven heaters in one thruster.

6.2 Leak testing

Leak testing on the feed system and thruster is so far done with gaseous nitrogen. The nozzle is closed off simply by applying a piece of tape. In the case of nitrogen leak tests, the purpose is to ensure correct nozzle mass flow measurements, in which case success is achieved if the leak rate is below the resolution of the mass flow sensor, which is about 10 $\mu g \cdot s^{-1}$. It is planned to be repeated with water in a similar way.

The feed system and thruster are pressurized to 4.5 bar and the mass flow is measured. This is shown in Fig. 14, where at t = 10 s the feed system starts pressurizing. Around t = 30 s the pressure is developed and mass flow drops to zero. Subsequently, around t = 40 s a leak is identified. This leak is found near the seal on the nozzle, which is tightened from t = 100 s onwards. As mass flow drops to below the resolution of the mass flow sensor, this result is currently sufficient.

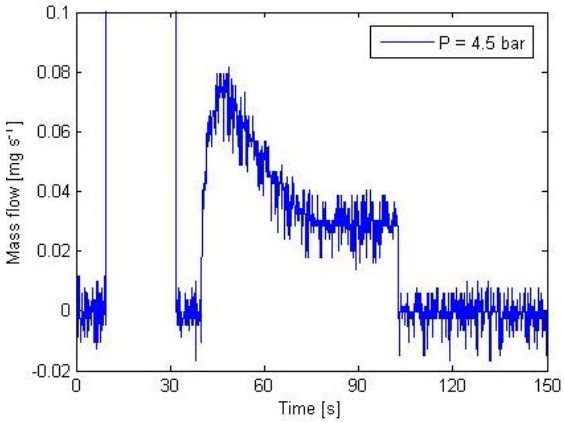

Figure 14. Results of leak test performed with nitrogen gas

6.3 Performance characterization

System performance testing focuses on determination of the nozzle quality and heating chamber efficiency. Furthermore, it aims to test the design on killer requirements such as structural integrity, circuit isolation etc. These tests require determination of the following parameters:

- Thrust force (F),
- Mass flow ($\dot{m}$),
- Chamber pressure (p_c),
- Chamber temperature (T_c),
- Dissipated power (P).

Test methods used to measure these and first test results are explained in the remainder of this section.

Thrust measurement

Thrust measurements on the VLM are to be performed with the AE-TB-5m test stand [17] available in the Delft Aerospace Rocket Thrust Stand (DARTS) facility at the Delft University of Technology. The AE-TB-5m has a vertical pendulum configuration and is shown in Fig. 15. The thrust delivered by a micro-propulsion system is determined by measuring the displacement of the pendulum arm induced by the thrust of the engine. The deflection of the pendulum is measured by means of a capacitive displacement sensor. The operational measurement range of this test stand configurable to the users need and is demonstrated between 1 µN to 15 mN with accuracies of 1% of the maximum measurement range. Other beneficial functionalities of this test stand are the operational capability in low vacuum conditions and an automated calibration process enabling consistent and reliable measurements uninfluenced by changing conditions between tests.

The measuring performance of the test stand is validated using the Bradford Engineering PMT [17] and the T^{3}µPS thruster used in the DUT Delfi-n3Xt CubeSat mission [18].
Fig. 16 shows a comparison of results obtained using the newly validated test stand (AE-TB-5m) and earlier results obtained with a different thrust balance (AE-TB-1.0). The data shows 10 measurement points for both the AE-TB-1.0 and the AE-TB-5m. The improvement in measurement precision of the AE-TB-5m can clearly be observed. It is quantified by the R^2 value of the fit, where a value of 0.996 is found for the AE-TB-5m and 0.973 for the AE-TB-1.0.

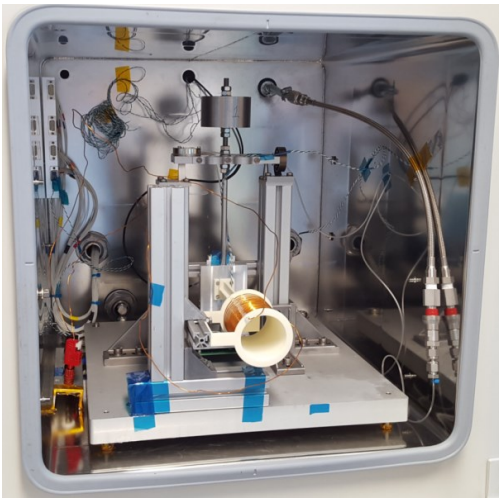

Figure 15. AE-TB-5m test stand inside a vacuum chamber

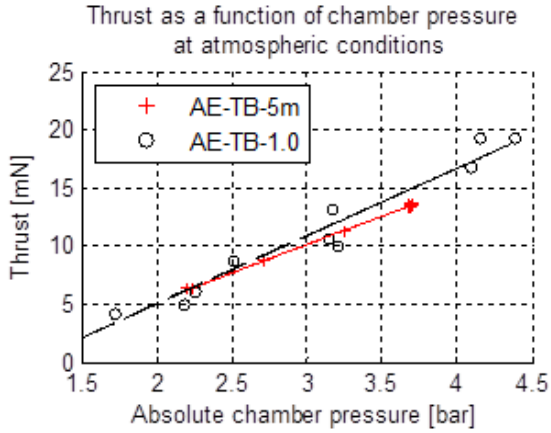

Figure 16. Thrust bench comparison when measuring the $T^3\mu PS$ – nozzle in cold gas mode

Mass flow measurement

In the first tests, only gaseous nitrogen is used as propellant. Nitrogen mass flow is directly measured using a mass flow sensor in the feed system. This has been used to determine the discharge coefficient of the nozzle in cold gas mode.
The discharge factor is determined by measuring mass flow of nitrogen gas, at a feed pressure of 4.5 bar in ambient temperature and pressure. The total pressure drop over the fluidic interface is conservatively estimated at 34 kPa. The throat area is found from Fig. 5.

The resulting worst-case discharge factor is found from eq. (1), which gives $C_d \geq 0.65$. This shows that the estimate of $C_D = 0.7$ used in the analytical model in Section is very reasonable. The design of the nozzle was based on [14], which also predicts a discharge coefficient of 0.7 for this nozzle.

In later tests, when liquid water is used as a propellant, tests are planned to be performed in blow-down mode instead and the mass flow is then determined by measuring the tank pressure. The process is planned as follows:

1. The tank and feed system are filled with propellant. A remainder of the volume is then filled with nitrogen pressurant, of which the mass is determined by integrating the mass flow signal.
2. The pressurant pressure is measured. From the pressure, temperature and mass of the pressurant, the volume is determined.
3. The tank and feed system are leak tested. They are pressurized and pressure is logged for two hours to ensure a minimal and, if any, well-determined leak rate.
4. During tests, the pressure will decrease as the pressurant expands. This is associated by an increase in volume, as a consequence of a decrease of propellant volume (i.e. mass).

Temperature measurement

The temperature sensing aims to determine the chamber temperature just prior to the nozzle. It is determined in three different ways, which are each indirect:

1. A thermocouple is applied to the outside top surface of the silicon thruster chip. This temperature is expected to be lower than the actual gas flow temperature at the nozzle inlet.
2. IV-curve method: The voltage and current on each heater is monitored, from which power and resistance follow. From the temperature coefficient of resistance (TCR), the temperature of the heater is then deduced. The TCR behavior of these SiC-heaters is described in [19]. By comparing the

temperature of the heater to the temperature just after t = 0, an additional increase in heater temperature is found. This rise is expected to correspond closely to the actual flow temperature.

3. When a stable choked flow exists in the nozzle, a temperature estimate is derived by comparing cold and hot mass-flow measurements. The temperature then follows from:

$$T_1 = T_2 \left(\frac{\dot{m}_1}{\dot{m}_2} \frac{p_{c2}}{p_{c1}} \frac{C_{D2}}{C_{D1}} \right)^2 \quad (7)$$

Here, T represents absolute temperature, $\dot{m}$ mass flow, p_c chamber pressure and C_D the discharge factor, while subscripts 1 and 2 represent hot and cold conditions, respectively.This method is expected to over-predict the chamber temperature, since it is based on the assumption of isentropic expansion, while heating of the flow still takes place in the convergent section of the nozzle.

Fig. 17 shows a typical test result obtained. It shows the resulting temperature estimates obtained using each method. In this experiment, a pressure of 4.5 bar is supplied in steady state and choked flow is maintained throughout the measurement. At t = 0 the heaters are powered at 1.3 W. As predicted, the thermocouple predicts the lower boundary while the mass-flow method predicts the upper boundary. From this measurement, an uncertainty of $\pm 10^{\circ}\mathrm{C}$ can be concluded. This can be reduced further with more accurate modeling.

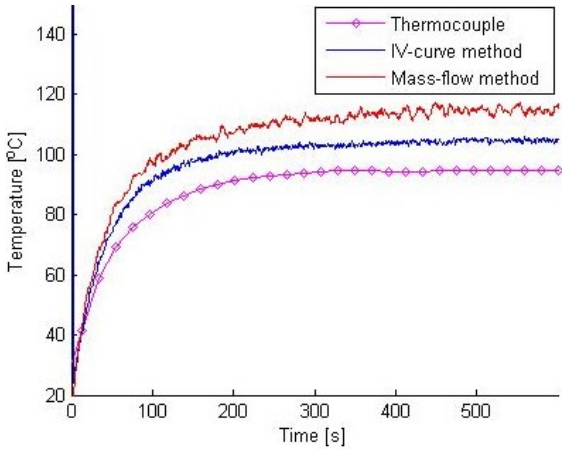

Figure 17. Temperature measured through three different methods

Pressure measurement

In order to determine the chamber pressure, ideally a sensor would be present inside the chamber. Since this is not feasible with the current system, it is measured in the feed system instead and the pressure drop over the feed system is estimated. In Section 5, it is already shown that the pressure loss in the chamber is negligibly small. The fluidic interface and inlet do have a significant pressure loss, which is estimated using the Darcy-Weisbach relation, which relates pressure drop (Δp) to the length (L), hydraulic diameter D_h, fluid density (ρ), fluid velocity (u) and a friction factor (f):

$$\Delta p = f \frac{L}{D_h} \frac{1}{2} \rho u^2 \quad (8)$$

The friction factor is a function of the local Reynold's number, the method to determine it is explained in [10]. Subtracting this pressure drop from the measured feed system pressure allows a reasonable estimate of the chamber pressure.

Power supply and measurement

Dissipated power is determined by measuring the current and voltage over each heater. Since the SiC-heaters have a negative temperature coefficient of resistance, the power has to be supplied in constant current mode. This requirement is supported by a constant voltage test, which clearly shows runaway behavior of the heater temperature. Constant current supply is achieved by means of implementing a current mirror, see Fig. 18 for the circuit diagram. This method allows measuring the current at one location, while the voltage drop over each heater is measured individually.

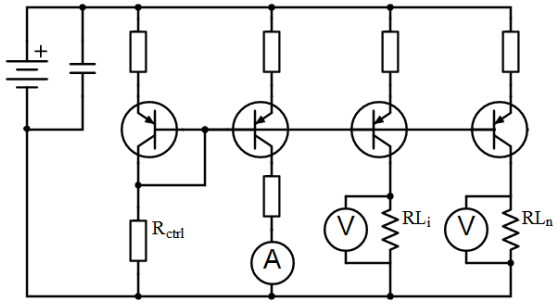

Figure 18. Circuit diagram of the current control circuit; all resistor-transistor pairs are identical. The left-most channel sets the current, which is then mirrored by the other transistors.

7 CONCLUSIONS

Significant advances are made in the development of the CubeSat micro-propulsion system at TU Delft. A breadboard version of the MEMS-VLM has been produced and subjected to

characterization and preliminary tests, on which valuable lessons have been learned on manufacturing, integration and testing.
An analytical steady-state model has been developed that allows to quickly and accurately investigate wall temperature requirements for new design proposals, which will be of great value for future updates to the design.
An engineering model design of the propellant storage tank is developed which is ready for production and testing.
Finally, a test plan and the test setup for the current breadboard model and future engineering models of the VLM is developed which allows thrust, mass flow, pressure, temperature and power to be determined.

The next step is to complete breadboard model testing of the MEMS-VLM. After that, future work focuses on updating the design of the current breadboard model to an engineering model, based on the lessons learned from breadboard testing. The focus of the engineering model design will shift more towards the packaging and integration of the MEMS-VLM into the propulsion system, where the thermal insulation and sealing of the interfaces are essential challenges.

8 REFERENCES

1. H. Heidt, J. Puig-Suari, A. Moore, S. Nakasuka and R. Twiggs. Cubesat: A new generation of picosatellite for education and industry low-cost space experimentation. In *Small Satellite Conference*, 2000.
2. W. Marshall and C. Boshuizen. Planet labs remote sensing satellite system. In *CubeSat Developers Workshop, 13-WK-15*, 2013.
3. A. Budianu, A. Meijerink and MJ Bentum. Swarm-to-earth communication in olfar. *Acta Astronautica*, 107: 14–19, 2015.
4. R. Poyck, I. Krusharev, B. Zandbergen, A. Cervone and Q. Bellini. Cubesat micro-propulsion systems for extending the capablities of academic projects. In *International Aeronautical Conference, Toronto, Canada*, 2014.
5. T.V. Mathew, B. Zandbergen, M. Mihailovic, J.F. Creemer and P.M. Sarro. A silicon-based mems-resistojet for propelling cubesats. In *Proceedings of the 62nd International Astronautical Congress*, 2011.
6. M. Mihailovic, T.V. Mathew, J.F. Creemer, B.T.C Zandbergen and P.M. Sarro. Mems silicon-based resistojet micro-thruster for attitude control of nano-satellites. In *IEE Solid-State Sensors, Actuators and Microsystems COnference*, 2011.
7. I. Krusharev, R. Poyck, Q. Bellini, B Zandbergen and A Cervone. Cubesat micro-propulsion systems for extending the capabilities of academic projects. In *International Astronautical Conference*, 2014.
8. R.M.A. Poyck. Design, manufacturing and characterisation of a water fed cuesat micro-resistojet - dondersteen. Master's thesis, Delft University of Technology, 2014.
9. G.P. Sutton. *Rocket Propulsion Elements*. John Wiley & Sons, Inc, 2001.
10. B. Zandbergen. *Thermal Rocket Propulsion*. TU Delft, 2016.
11. J.W. Cen and J.L Xu. Performance evaluation and flow visualization of a mems based vaporizing liquid micro-thruster. *Acta Astronautica*, 67: 468–482, 2010.
12. C.C. Chen, C.W. Liu, H.C. Kan, L.H. Hu, G.S. Chang, M.C. Cheng and B.T. Dai. Simulation and experiment research on vaporizing liquid micro-thruster. *Sensors and Actuators A*, 157: 140–149, 2010.
13. T. Bergman, A. Lavine, F. Incropera and P. Dewitt. *Chemie Ingenieur Technik, 7th edition*. WILEY-VCH Verlag GmbH & Co. KGaA, Weinheim, 2011.
14. F. La Torre. *Gas Flow in Miniaturized Nozzles for Microthrusters*. PhD thesis, Delft University of Technology, 2011.
15. P. Kundu, T. K. Bhattacharyya and S. Das. Design, fabrication and performance evaluation of a vaporizing liquid microthruster. *Journal of Micromechanics and Microengineering*, 22, 2012.
16. I. Granero, E. Jansen, T. van Wees, A. Cervone and B. Zandbergen. Design trades applied to a propellant tank for a water resistojet. 2016.
17. R.J.F. Bijster. Design, verification and validation of a micropulsion thrust stand. Master's thesis, Delft University of Technology, 2014.
18. S. De Jong, E. Maddox, G.J. Vollmuller, W.J. Ubbels and R.J. Hamann. The delfi-n3xt nanosatellite: Space weather research and qualitification of microtechnology. In *59th International Astronautical Congress, Glasgow*, 2008.
19. B. Morana, F. Santagata, L. Mele, M. Mihailovic, G. Pandraud, J.F. Creemer and P.M. Sarro. A silicon carbide mems microhotplate for nanomaterial characterization in tem. *Proceedings of the IEEE, Cancun, Mexico*, pages 380–383, 2011.